Electronic and Magnetic Properties of Hybrid Boron Nitride Nanoribbons and Sheets with 5–7 Line Defects

ARTICLE *in* THE JOURNAL OF PHYSICAL CHEMISTRY C · AUGUST 2013

Impact Factor: 4.77 · DOI: 10.1021/jp405536x

2 AUTHORS, INCLUDING:

Shaobin Tang
Xiamen University
21 PUBLICATIONS **342** CITATIONS

SEE PROFILE

THE JOURNAL OF PHYSICAL CHEMISTRY C

Article

pubs.acs.org/JPCC

Electronic and Magnetic Properties of Hybrid Boron Nitride Nanoribbons and Sheets with 5−7 Line Defects

Shaobin Tang* and Shiyong Zhang

Key Laboratory of Organo-Pharmaceutical Chemistry of Jiangxi Province, Gannan Normal University, Ganzhou 341000, China

Supporting Information

ABSTRACT: The first-principles calculations have been used to investigate the electronic and magnetic properties of hybrid boron nitride nanoribbons (BNNR) and sheets, which are constructed by the B-rich or N-rich grain boundaries (GB) with the pentagon−heptagon (5−7) line defect joining together the normal zigzag and armchair BN segments. Our results show that, in contrast to the pristine BN systems, the hybrid BN nanostructures with 5−7 line defects possess some unique electronic and magnetic properties. The hybrid BNNR with H-passivated edge and BN sheet are semiconductors with notably reduced band gap due to the presence of line defect state, as compared to the normal BN systems. The band gaps of H-passivated hybrid BNNR with B-rich and N-rich GB exhibit the different variation with the ribbons width. The hybrid BNNR created by B-rich GB with bare N edge for all widths are half-semiconductors with the ferromagnetic ground state, whereas for the hybrid BNNR with bare zigzag B edge the antiferromagnetic → nonmagnetic semiconductor transition occurred when its narrow zigzag segment is changed to the wider one. Interestingly, totally different from the perfect zigzag BNNR, the hybrid BNNR with two-H-terminated B edge exhibit the metallic → half-semiconducting → half-metallic behavior transitions as its number of zigzag BN chains gradually increases due to the compressed zigzag edge. Therefore, the hybrid BN nanostructures constructed by GB with 5−7 line defects may provide potential applications for BN-based nanoelectronic and spintronic devices.

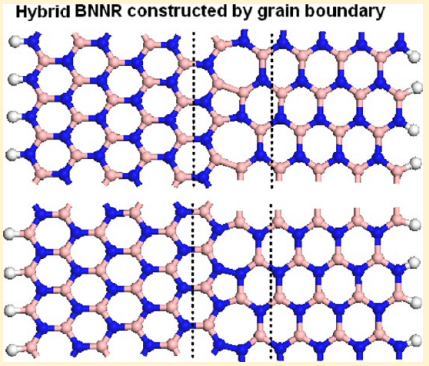

1. INTRODUCTION

Two-dimensional (2D) hexagonal boron-nitride (*h*-BN) sheets, structural analogues of graphene, have attracted immense interest due to their high chemical stability and remarkable properties.[1−5] Graphene is a semimetal with a zero band gap, whereas the *h*-BN sheets are wide-band gap semiconductors. The realization of BN-based nanomaterials with tunable band gaps smaller than 3 eV is highly desirable for potential application in nanoelectronics and optoelectronics. Many methods are proposed to reduce the band gap of *h*-BN, such as full hydrogenation or fluorination[6−8] and cutting *h*-BN into nanoribbons.[9,10]

Boron nitride nanoribbons (BNNRs) can present fascinating electronic and magnetic properties depending on the ribbon sizes and edge shape as well as edge termination.[11−19] Previous theoretical works show that band gaps of zigzag BNNR (ZBNNR) with H-saturated edge, which are reduced with increasing ribbons width, are well modulated by an external transverse electric field[11,12] and by uniaxial tensile strain.[13] Interestingly, in the absence of electric field, the half-metallic properties are found in ZBNNR with one bare N edge and one H-terminated B edge[14,15] and with partial hydrogenation[16] or edge fluorination.[17] Furthermore, our previous works reveal that carbon chain-doped ZBNNR may produce half-semiconducting → half-metallic → metallic behavior transitions without the external electric field.[20]

Grain boundaries (GB) in polycrystalline graphene play an important role in determining the electronic and magnetic properties and transport property of graphene-based materials, and therefore have been extensively studied in recent years. Recently, the experiment works by Lahiri et al. report[21] the realization of one-dimensional extended topological defect in graphene, containing the pentagon−octagon−pentagon (5−8−5) line defect embedded in perfect graphene sheet. It is suggested that such a defect in graphene acts as a quasi-one-dimensional metallic wire. The GB structure-dependent electron transport behaviors in graphene are found.[22] Ab initio calculations[23] indicate that the translational grain boundary in graphene leads to the magnetic states strongly confined to the core of the defect, which are protected from the contamination and reconstruction effects. In particular, the periodical GB with pentagon-heptagon (5−7) line defect can be used to join the normal zigzag and armchair graphene nanoribbons (GNRs) to form hybrid GNRs. The first-principles calculations show that the hybrid GNRs can exhibit interesting electronic and magnetic properties, totally different from those of normal GNRs.[24,25]

Similarly, when *h*-BN sheets are prepared by chemical vapor deposition (CVD) on metal substrate, the polycrystalline BN

Received: June 4, 2013
Revised: August 1, 2013
Published: August 1, 2013

dx.doi.org/10.1021/jp405536x | J. Phys. Chem. C 2013, 117, 17309−17318

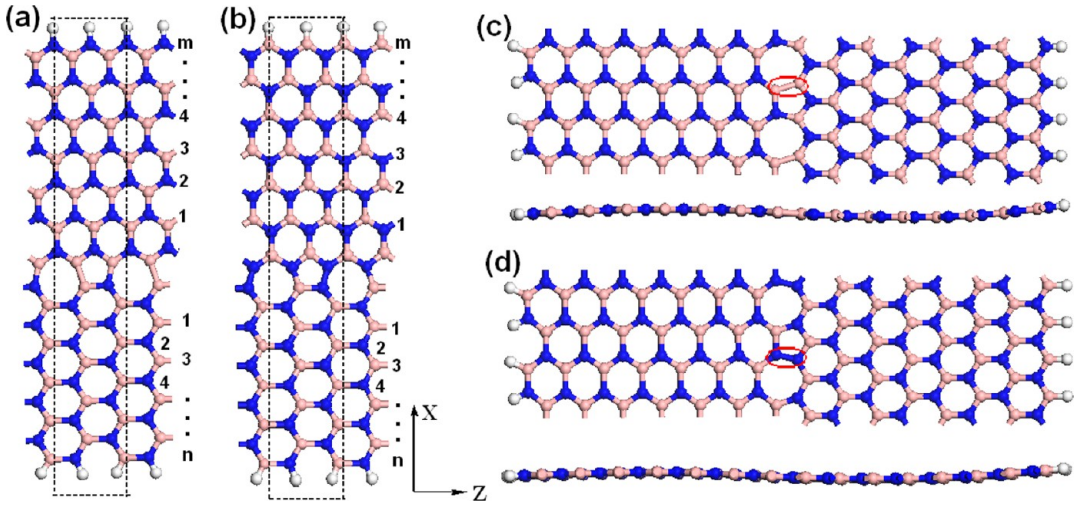

Figure 1. Schematic structures of hybrid BNNRs constructed by (a) B-rich GB and (b) N-rich with 5−7 line defects, which are arranged alternatively along the *z* direction. The *m* and *n* in (a) and (b) denote the widths of the zigzag and armchair sections in hybrid ribbons, respectively, and the dashed rectangles represent the unit cell of hybrid BNNRs. Top and side views of optimized structures of (c) HN-Z7-A12-BNNR and (d) HB-Z7-A12-BNNR. The homoelemental B−B in (c) and N−N bonds in (d) are marked by red circles. The H, N, and B atoms are denoted by white, blue, and light pink balls, respectively.

sheets can be formed,[26,27] where two growth fronts with B- or N-terminated edges meet each other, leading to B-rich or N-rich GB. Using the first-principles calculations, Yakobson et al.[28] suggest that the GB structures in *h*-BN can consist of either a polar B-rich (N-rich) 5−7 pair with homoelemental B−B (N−N) bonds or an unpolar square-octagon pair (4−8), depending on the tilt angle of grains. Furthermore, the ab initio calculations[29] indicate that the structures of antiphase boundaries (APBs) with armchair and zigzag chiralities in monolayer BN are strongly determined by the chemical potentials of boron (B) and nitrogen (N) in the synthesis process. On the basis of the first-principles calculations and Born−Oppenheimer quantum molecular dynamic simulation (BOMD), it is reported that pentagon−octagon−pentagon (5−8−5) line defects can be created in the ZBNNR and BN sheet, possessing some unique eletronic and magnetic properties.[30] Recently, the spin-polarized first-principles calculations[31] show that the zigzag BNNR with pentagon−heptagon line defect at a single edge as well as at both edges can present the interesting antiferromagnetic half-metallic behavior when the number of this line defect is even.

Similar to hybrid graphene systems, the hybrid BNNR and sheet with normal zigzag and armchair BN segments may be constructed by GB with the 5−7 line defect. The novel physical and chemical properties in such systems, different from those of perfect BN, are expected due to the existence of the GB. In this Article, we report the first-principles calculations on the electronic and magnetic properties of hybrid BN nanoribbons and sheets with both zigzag and armchair segments, which are joined by the 5−7 line defect. Our results show that the 5−7 line defects in hybrid BN ribbons reduce the band gaps of perfect BN systems, and the hybrid BN nanoribbons with two-hydrogen-terminated zigzag B edge exhibit metallic → semiconducting → half-metallic behavior transitions as the number of zigzag BN chains increases.

2. COMPUTATIONAL DETAILS

All calculations in this work have been performed by using the plane-wave technique implemented in the Vienna ab initio simulation package.[32] The projector augmented wave method (PAW)[33] was used to describe the electron−ion interaction. A plane wave basis set with a cutoff energy of 400 eV was used for the electron wave function. The generalized gradient approximation (GGA) in the Perdew−Burke−Ernzerhof[34] form is employed to describe the exchange-correction potential for the spin-polarized and spin-unpolarized calculations. The 1D and 2D periodic boundary conditions are considered along the growth directions of nanoribbons and sheets, respectively. Vacuum spacings larger than 10 Å for sheet and 12 Å for nanoribbon edges between periodic cells were used in the calculations. Monkhost−Pack meshs of *k*-points 1 × 1 × 13 and 3 × 1 × 7 were used for sampling the 1D and 2D Brillouin zones during the geometry optimization, respectively. All atomic positions were optimized by the conjugate gradient method with the converging tolerance of 0.02 eV/Å for the forces on all atoms. The convergence criterion of energy for self-consistent field computations is 10^{-5} eV. The electronic structure calculations were preformed by using 21 *k*-points along the periodic orientation. To investigate the stability of hybrid BN nanoribbons, the ab initio molecular dynamics (AIMD) simulations are carried out in the canonical ensemble at different temperatures of T = 300, 600, and 1000 K. In AIMD simulations, the nanoribbon supercell containing two unit cells is used, and the time step is set to 1 fs.

In calculated models, as shown in Figure 1, the hybrid BNNRs are constructed by GB with a linear array of pentagon and heptagon rings, called a 5−7 line defect, which connects the armchair nanoribbon at one side and the zigzag nanoribbon at the other side. Because of the presence of both B- and N-terminated edges in normal ZBNNR, when zigzag and armchair nanoribbons meet each other to form hybrid BNNR, there are two types of 5−7 defect: one is the B-rich GB with homoelemental B−B bonding (Figure 1a), and the other is the N-rich GB with homoelemental N−N bonding (Figure 1b). Accordingly, the hybrid BN ribbons with B-rich (N-rich) 5−7 defect lead to the N-terminated (B-terminated) zigzag edge, defined as N-BNNR (B-BNNR). Following the previous convention,[35−37] the geometrical structures of hybrid BNNR

dx.doi.org/10.1021/jp405536x | J. Phys. Chem. C 2013, 117, 17309−17318

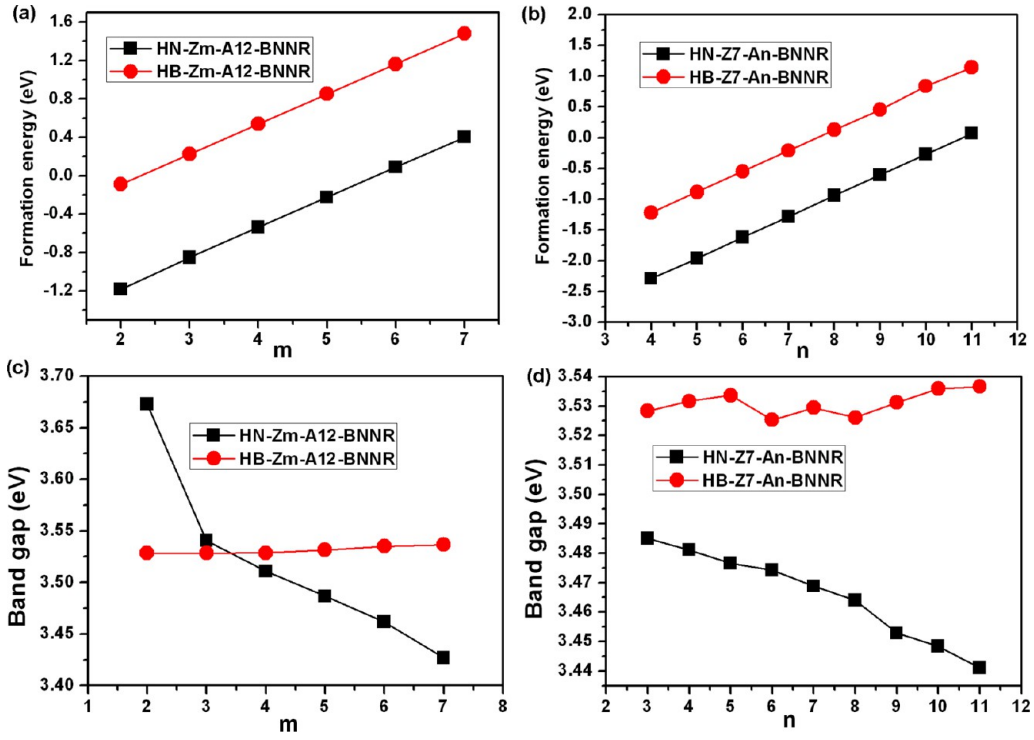

Figure 2. Formation energy and band gap of hybrid BN nanoribbons as a function of width of zigzag and armchair segments. (a and c) HN-Z*m*-A12-BNNR and HB-Z*m*-A12-BNNR, (b and d) HN-Z7-A*n*-BNNR and HB-Z7-A*n*-BNNR.

with different widths are identified by N/B-Z*m*-A*n*-BNNR (Figure 1a and b), where *m* and *n* represent the numbers of zigzag and armchair BN chains along its width direction, respectively. When the zigzag N or B edges are bare, and passivated by one and two hydrogen atoms, the hybrid nanoribbons are denoted as N/B-Z*m*-A*n*-BNNR, HN/B-Z*m*-A*n*-BNNR (Figure 1), and 2HN/B-Z*m*-A*n*-BNNR, respectively. In all cases, the armchair edges in hybrid BNNR are passivated by H atoms.

3. RESULTS AND DISCUSSION

3.1. Hybrid BNNR with H-Terminated Edge. We first discuss the geometrical structures of hybrid BNNR constructed by the B-rich or N-rich GB with H-terminated zigzag edge. Figure 1c and d shows the optimized structures of HN-Z7-A12-BNNR and HB-Z7-A12-BNNR, respectively. The short distance between two nearest-neighboring N (B) atoms of 1.43 Å (1.67 Å) in 5−7 line defects indicates the formation of homoelemental N−N (B−B) bonds. Different from the normal BNNR, the presence of B-rich or N-rich GB with 5−7 line defect in hybrid BN ribbons leads to slight out-of-plane structural distortion of zigzag and armchair segments along its width direction (side view in Figure 1c and d), which may effectively relax the strain from defect core. Our calculations show that such distortion for hybrid ribbons with larger width becomes more prominent than the narrow one. The lattice mismatches between hybrid BNNR and normal zigzag and armchair BNNR are found to be −5% and 7.9%, respectively, suggesting that the zigzag segment is compressed and the armchair section is elongated. Similar results are reported by previous first-principles calculations on hybrid GNR.[24,25]

To investigate the thermodynamic stability of hybrid BN nanoribbons, the formation energy is calculated by $E_f = E_{H-BN} - n_N\mu_N - n_B\mu_B - n_H E_{H_2}/2$, where E_{H-BN} and E_{H_2} are the total energies of hybrid BN nanoribbons and free hydrogen molecule, respectively, n_i (i = N, B, and H) is the number of i atoms, and μ_i is the corresponding chemical potential. Because the *h*-BN sheet is used as the precursor material of hybrid BN ribbons, we choose $\mu_B + \mu_N$ as the binding energy per BN pair of *h*-BN sheet. It is noted that the hybrid BN ribbons with the negative formation energies exhibit higher stability than its constituents. Figure 2a and b presents the formation energies of HN/B-Z*m*-A12-BNNR and HN/B-Z7-A*n*-BNNR as a function of width of zigzag and armchair segments, respectively. Clearly, the formation energies of hybrid BNNR with B-rich or N-rich GB monotonically increase with increasing ribbons width, suggesting that the narrow ribbons are more likely accessible than the wider one. As shown in Figure 2a and b, the hybrid nanoribbons created by the B-rich 5−7 line defect (black line) are energetically more stable than that of ribbons with N-rich GB (red line) in the case of the same width. Such width-dependent stabilities differ from the hybrid graphene nanoribbons,[24] where the stability of ribbons increases with increasing width. In addition, the bond energies per N−H (B−H) in zigzag edge for HN/B-BNNR are evaluated to be 5.15 eV (4.55 eV), suggesting that the binding of hydrogen to the zigzag section edges is thermodynamically stable.

To further investigate the stability of hybrid BN nanoribbons constructed by 5−7 line defect, we perform AIMD simulations on HN-Z3-A5-BNNR and HB-Z3-A6-BNNR at different temperatures of 300, 600, and 1000 K. As shown in Figure 3 and Supporting Information Figure S1, after running 2000 steps, the 5−7 line defects of B-rich GB and N-rich GB in hybrid BNNR still remain as compared to the initial structures even at a high temperature of 1000 K, although the planar structure of ribbon exhibits some structural distortion. In addition, the stability of hybrid BN nanoribbon is also confirmed by our subsequent 3 ps simulation at a temperature

dx.doi.org/10.1021/jp405536x | J. Phys. Chem. C 2013, 117, 17309−17318

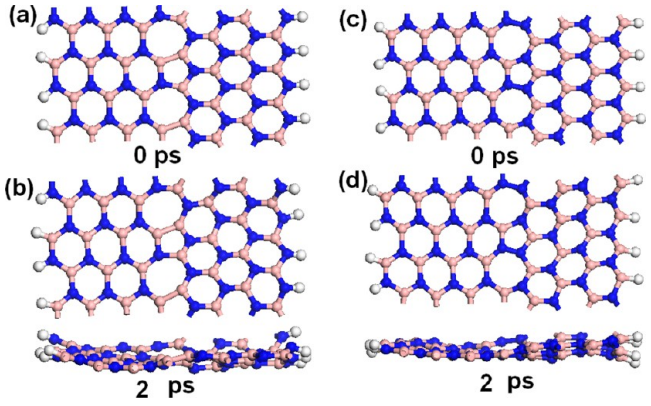

Figure 3. Geometrical structures of hybrid BNNRs with 5−7 line defects at the simulation times 0 and 2 ps under the temperature 1000 K. (a and b) HN-Z3-A5-BNNR, (c and d) HB-Z3-A6-BNNR.

of 1000 K (see Figure S1d in the Supporting Information). This simulation results show that the hybrid BN nanoribbons created by 5−7 line defect are stable.

We now discuss the electronic properties of hybrid BN nanoribbons with H-terminated zigzag edge. Figure 4a and d displays the band structures of HN-Z5-A12-BNNR and HB-Z5-A12-BNNR, respectively. The calculated results show that the two hybrid BN ribbons created by B-rich and N-rich GB are semiconductors with indirect or direct band gaps of 3.48 and 3.53 eV, respectively, which are reduced as compared to 4.05 eV (4.47 eV) of perfect zigzag (armchair) BNNR with the same ribbon width at the same level. The smaller band gaps in hybrid BNNR than in perfect BNNR are also found for all other ribbon widths. To illustrate the mechanism for reducation of band gap, the partial charge densities of valence band maximum (VBM) and the conduction band minimum (CBM), total density of states (DOS), and the projected density of states (PDOS) for HN-Z5-A12-BNNR and HB-Z5-A12-BNNR are depicted in Figure 4b, c, and e−h. The calculated PDOS (Figure 4g and h) clearly show that the 5−7 line defects lead to the defect state with large dispersion within the band gap of perfect BNNR. The electronic states in VBM for N-BNNR with H-passivated zigzag edge are mainly contributed by p_y orbitals of N atoms from zigzag segment (Figure 4b and g), whereas the CBM mainly consists of the homoelemental B−B bond in 5−7 defects (Figure 4c and g). In the case of hybrid BN ribbons with N-rich GB, the electronic states in VBM and CBM are mainly contributed by the N and B atoms from 5−7 line defect (Figure 4e, f, and h), respectively. Therefore, the presence of defect states may be responsible for the reduced band gap. Similar defect sates are found in line defect-embedded BN nanoribbons.[30]

The dependence of semiconducting band gap on the zigzag width *m* for HN/B-Z*m*-A12-BNNR and on the armchair width *n* for HN/B-Z7-A*n*-BNNR is investigated. Figure 2c and d presents the change of band gaps with ribbons width *m* and *n*. For the hybrid nanoribbons with homoelemental B−B bond, the band gaps of HN-Z*m*-A12-BNNR (HN-Z7-A*n*-BNNR) decrease from 3.672 to 3.426 eV (3.485 to 3.441 eV) with increasing width *m* from 2 to 7 (*n* from 3 to 11). In the case of N-rich GB, however, the band gaps of hybrid BN nanoribbons (red lines in Figure 2c and d) are found to be less dependent

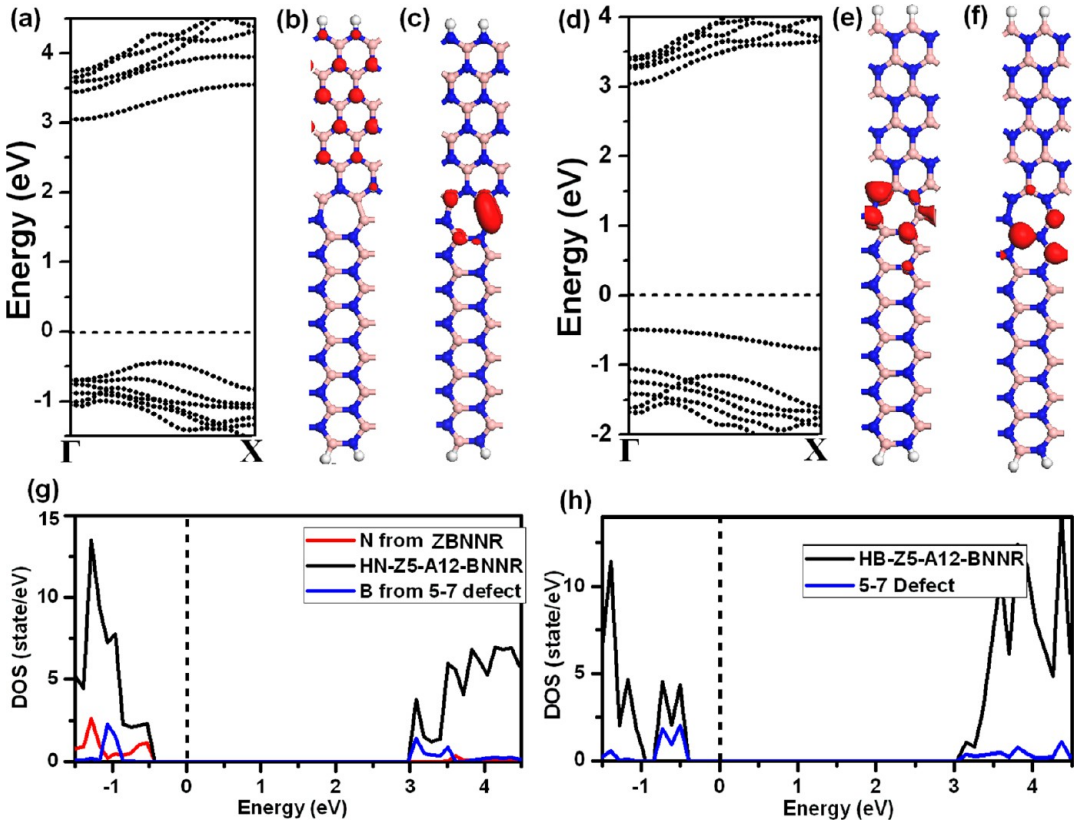

Figure 4. Band structures (a), partial charge densities of (b) VBM and (c) CBM, and total DOS (g) of HN-Z5-A12-BNNR. The isosurface in (b) and (c) is 0.02 e/Å^3. The (d)−(f) and (h) for HB-Z5-A12-BNNR are similar to (a)−(c) and (g), respectively. The PDOS of (g) B atoms from 5−7 defect and N from zigzag section in HN-Z5-A12-BNNR and (h) 5−7 defect in HB-Z5-A12-BNNR are shown.

dx.doi.org/10.1021/jp405536x | J. Phys. Chem. C 2013, 117, 17309−17318

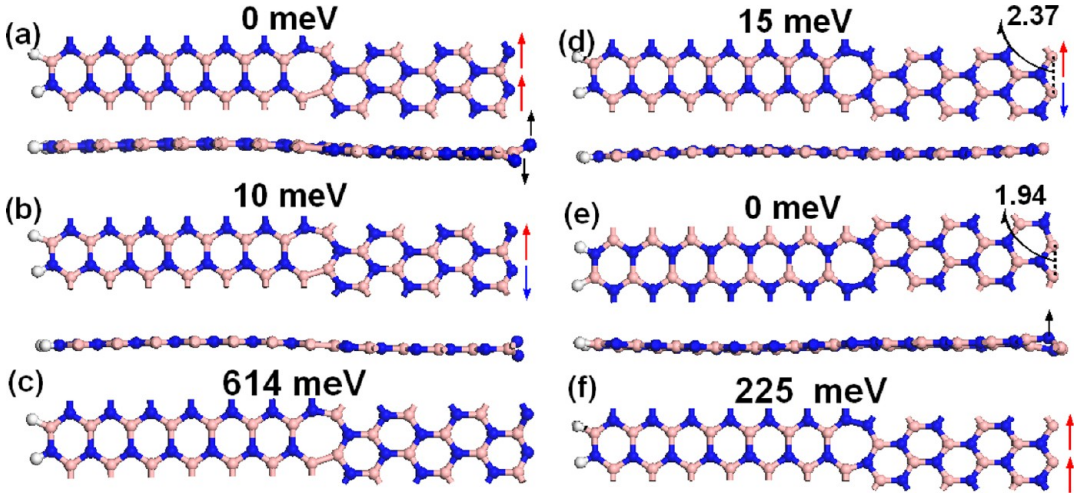

Figure 5. Optimized structures of (a)−(c) N-Z5-A12-BNNR and (d)−(f) B-Z5-A12-BNNR in the FM, AFM, and NM states. (a and f) FM state, (b and d) AFM state, and (c and e) NM state. The red up and blue down arrows at the edge atoms denote the spin-up and spin-down directions, respectively. The black arrows in side view of (a) and (e) show the distortion direction of N atoms relative to the plane structure. The relative energies per unit cell for various states with respect to the ground state are shown, and distances between edge B atoms are in angstroms.

on the width, although the armchair segment width n has a small impact on the band gap of HB-Z7-An-BNNR. The present results are totally different from the perfect zigzag and especially from the armchair BNNR. Because of the quantum confinement effect, the band gaps of perfect armchair BNNR[11,12] and GNR[38] show a family behavior of 3p (p is an integer). Such band gap change of hybrid BNNR with ribbon width can be explained by the partial charge densities of VBM and CBM. For the hybrid BN ribbons with N-rich GB (HB-Zm-An-BNNR), the presence of defect states (Figure 4e and f) determining the band gap instead of the edge state for perfect ABNNR may be responsible for the less width-dependent band gap. In contrast, for ribbons with B-rich GB, the electronic states of CBM in HN-Zm-A12-BNNR are mainly controlled by N atoms in zigzag segment decaying from interior domain to two zigzag edges, resulting in the decrease of band gap with increasing ribbon width m.

3.2. Hybrid BNNR with Bare N and B Edges. Previous theoretical results[14,15,18] show that the full-bare edges and half-bare N or B edges in zigzag BNNR can present various spin configurations, and interesting magnetic and electronic properties are found in those bare zigzag BNNR. Here, we discuss the magnetic and electronic properties of hybrid BN ribbons with bare zigzag edge. As shown in Figure 5, two bare N atoms (B atoms) in zigzag edge of N-BNNR (B-BNNR) with one unit cell can present the antiferromagnetic (AFM) or ferromagnetic (FM) spin alignment. To determine the ground state, we perform the spin-polarized and spin-unpolarized calculations on N/B-Zm-An-BNNR. The geometrical structures of hybrid BNNR in all of these states are first discussed. Figure 5 displays the optimized structures of N/H-Z5-A12-BNNR in the AFM and FM states and nonmagnetic (NM) state. After geometry optimization, two bare edge N atoms in N-Z5-A12-BNNR slightly move out of the ribbon plane in opposite directions due to the compressed zigzag edge regardless of the AFM, FM, and NM states (Figure 5a−c). For hybrid B-BNNR with bare B edge, however, the spin-polarized and spin-unpolarized calculations lead to the different local edge structures. As shown in Figure 5d,e, the planar edge structure in B-Z5-A12-BNNR is well remained in the AFM and FM states, whereas for the NM state the distance between two edge B atom is shortened from 2.37 to 1.94−2.02 Å depending on the zigzag width (Figure 5d and e), giving rise to a NH_3-like N structure with two nearest-neighbor edge B atoms. Such distorted edge structures are different from the perfect ZBNNR with the same bare edges.[14,15,18]

Table 1 and Figure 5 display the relative energies of AFM and FM states and nonmagnetic (NM) state of B/N-Zm-An-BNNR. The FM state of N-Zm-A12-BNNR (m = 4, 5, and 7) is 10 and 614−625 meV per unit cell lower in energy than the AFM and NM states, respectively, indicating the ferromagnetic ground state. The electronic property of the FM ground state is unaffected by the armchair segment n (Table 1). The small energy difference of 10 meV per unit cell between AFM and FM states shows that two spin-polarized states in hybrid BN nanoribbons with bare N edge are thermally accessible at room temperature (26 meV). Qualitatively different from the half metallic properties for perfect ZBNNR with bare N edge and H-terminated B edge,[14,15] band structure calculations (Figure 6a and Figure S2 in the Supporting Information) show that the hybrid BNNR with bare N edge in the ground state are half-semiconductors, in which two spin semiconducting channels

Table 1. Relative Energies (meV/unit cell) of Antiferromagnetic (AFM), Ferromagnetic (FM), and Spin-Unpolarized (NM) States of B/N-Zm-An-BNNR with Various m and n Values[a]

structures	AFM	FM	NM
N-Z4-A12-BNNR	10	0	625
N-Z5-A12-BNNR	10	0	614
N-Z7-A12-BNNR	10	0	620
N-Z4-A7-BNNR	10	0	628
B-Z3-A12-BNNR	0	224	55
B-Z4-A12-BNNR	0	225	97
B-Z4-A8-BNNR	0	224	94
B-Z5-A12-BNNR	15	210	0
B-Z7-A12-BNNR	16	209	0
B-Z9-A12-BNNR	24	201	0
B-Z6-A10-BNNR	12	213	0

[a]The energy of the ground state is set to 0.

dx.doi.org/10.1021/jp405536x | J. Phys. Chem. C 2013, 117, 17309−17318

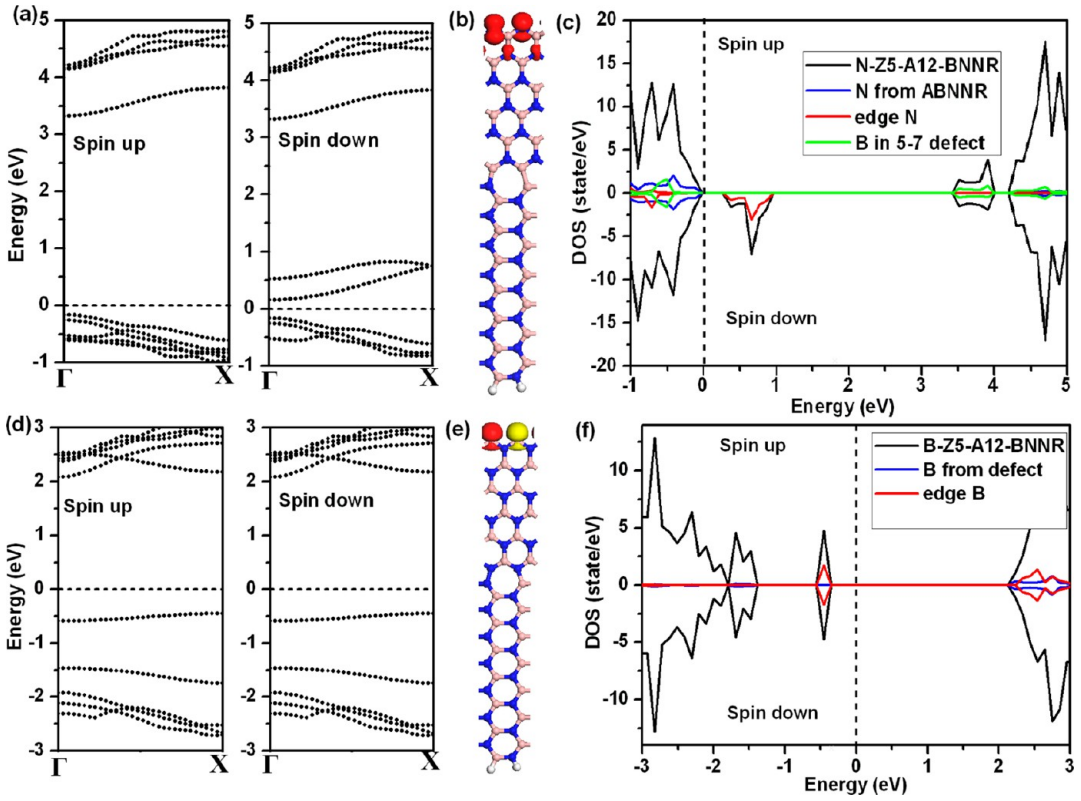

Figure 6. Band structures, spin densities, and total DOS of (a)−(c) N-Z5-A12-BNNR in the FM state and (d)−(f) B-Z5-A12-BNNR in the AFM state. The isosurface in (b) and (e) is 0.05 e/Å^3 with red for spin up and yellow for spin down. The PDOS of different (c) N and B atoms in N-Z5-A12-BNNR and (f) B atoms in B-Z5-A12-BNNR are shown. The Fermi level is set to 0.

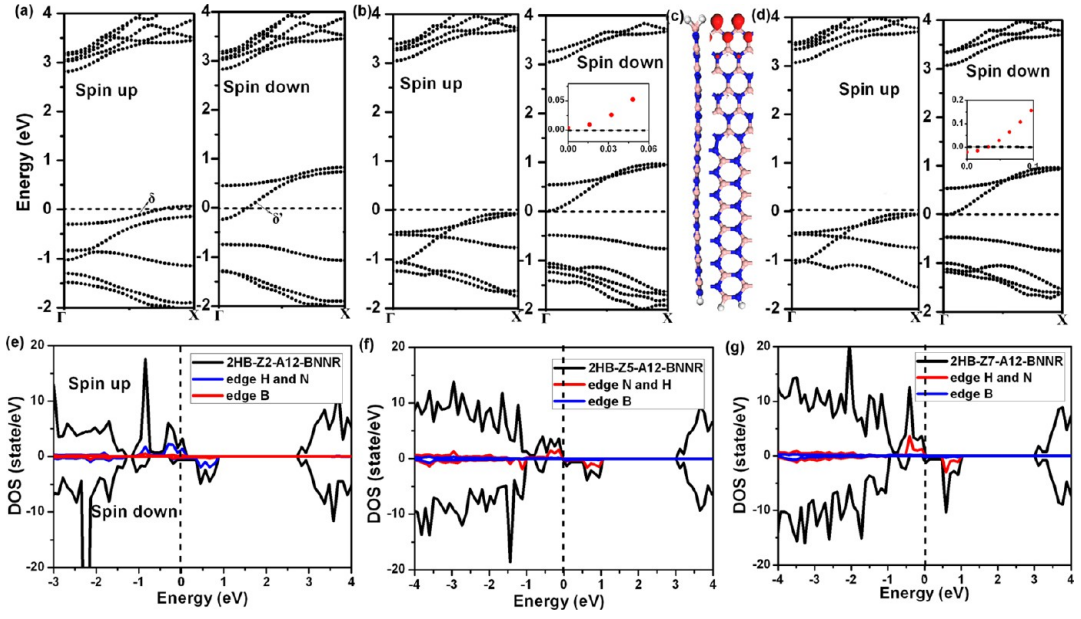

Figure 7. Band structures and total DOS of (a and e) 2HB-Z2-A12-BNNRs, (b and f) 2HB-Z5-A12-BNNRs, and (d and g) 2HB-Z7-A12-BNNRs, respectively. The insets in the right panel of (b) and (d) are the band structures near the Fermi level. PDOS of H-terminated B, and N and H atoms connecting the edge B of hybrid ribbons in (e)−(g) are also shown. (c) The side view of optimized structure (left panel) and spin densities (right panel) of 2HB-Z5-A12-BNNRs: the isosurface is 0.05 e/Å^3 with red for spin up and yellow for spin down. The Fermi level is set to 0.

have different band gaps. For example, as shown in Figure 6a, the spin-up channel for N-Z5-A12-BNNR has a direct band gap of 3.48 eV, while the value for the spin-down channel becomes 0.32 eV. On the basis of the partial charge densities (see Figure S3a−3d in the Supporting Information), although the electrons from VBM are almost degenerate for two spin channels, which have the same contribution by N atoms from armchair segments, the electronic states of CBM for spin-up and spin-down channels mainly come from the B atoms in 5−7 defect and edge N atoms, respectively, giving rise to the different band

dx.doi.org/10.1021/jp405536x | J. Phys. Chem. C 2013, 117, 17309−17318

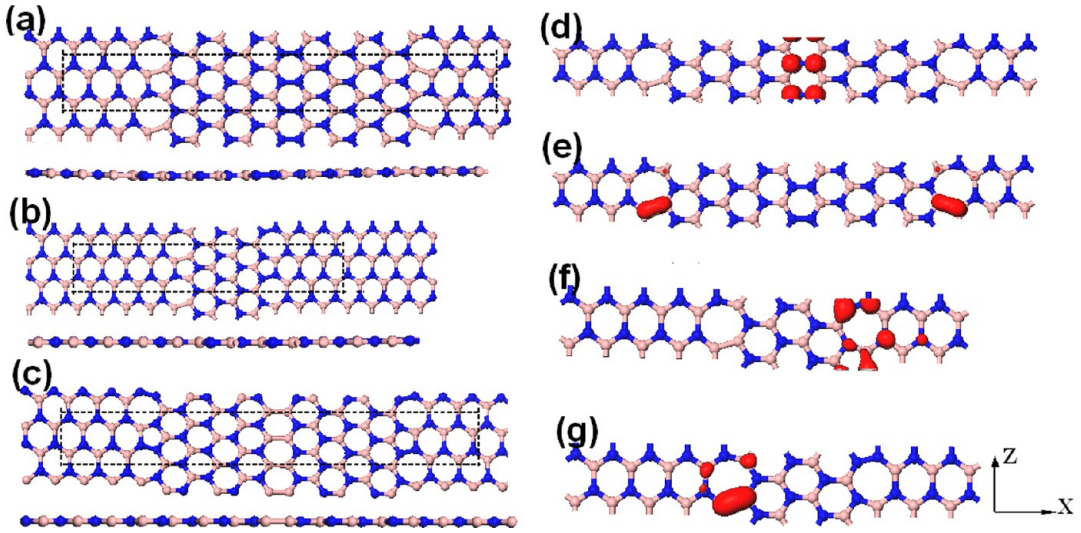

Figure 8. Schematic structures (top view) of 2D hybrid BN sheet constructed by (a) both B-rich 5−7 defect and N antisite line defects, (b) both B-rich and N-rich 5−7 defects, and (c) both N-rich 5−7 defect and B antisite line defects. The dashed rectangles denote the unit cell of hybrid BN sheet, and the side view of the corresponding geometrical structures is also shown in (a)−(c). Partial charge densities of (d,f) VBM and (e,g) CBM of hybrid BN sheet with (d,e) BG-N2-BN and (f,g) BG-NG-BN. The isosurface is 0.02 e/Å^3. Note that the growth directions of BN sheet are along *x* and *z*.

gap in two spin channels. The spin densities and DOS and PDOS for N-Z5-A12-BNNR (Figure 6b and c) show the ferromagnetic ground state leads to a magnetic moment of 1 μ_B per edge atom, which is mainly located at zigzag edge N.

In contrast to N-BNNR, as shown in Table 1 and Figure 5, when the B edge of hybrid BNNR constructed by N-rich 5−7 defect is bare, the B-Z*m*-A12-BNNR with narrow zigzag section (m = 3 and 4) has an antiferromagnetic ground state, whereas it becomes nonmagnetic state with increasing zigzag width (m = 5−9). The NM ground state of B-BNNR may be ascribed to the structural distortion of bare zigzag B edge (Figure 5e). For the B-BNNR with larger width of zigzag section, although the NM state is energetically more stable than the AFM state (Table 1), the small energy difference of 6−12 meV per edge atom between AFM and NM states as compared to that at room temperature (26 meV) suggests that such hybrid ribbons can exhibit antiferromagnetic behavior at room temperature. From Table 1, the AFM or NM ground state of B-Z*m*-A*n*-BNNR is mainly determined by the zigzag segment width, but less affected by the armchair domain width.

The electronic structure calculations (Figure 6d and Figure S4 in the Supporting Information) show that the B-Z*m*-A12-BNNR in the AFM and NM states are semiconductors. As an example, the band structures of B-Z5-A12-BNNR in the AFM state are shown in Figure 6d. The electronic states for two spin channels are degenerated with an indirect band gap of 2.53 eV, which is mainly determined by the B atoms in zigzag edge and by the interface B atoms between 5 and 7 defect and armchair domain based on the DOS and PDOS (Figure 6f) and the partial charge densities (Figure S3e and S3f in the Supporting Information). The spin densities (Figure 6e) of B-Z5-A12-BNNR clearly show that the antiparallel spin alignment is mainly localized at the bare B atoms, leading to zero net magnetic moment. Such semiconducting properties of hybrid BNNR in the AFM state are similar to those of perfect ZBNNR with the same bare edge.[14,15]

3.3. Hybrid BNNR with Two Hydrogen-Terminated Zigzag B Edge. We now investigate the effect of B edge passivation by two hydrogen on electronic and magnetic properties of the hybrid BNNR with N-rich GB (B-BNNR). We first determine the ground state of B-BNNR with two H-terminated B edge (2HB-BNNR) using the spin-polarized and spin-unpolarized calculations. The ferromagnetic state of 2HB-BNNR is 53 meV per edge atom lower in energy than the nonmagnetic state regardless of the zigzag segment width, suggesting the FM ground state. In view of the thermal energy at room temperature (26 meV), the two hydrogen-passivated B-BNNR will maintain the ferromagnetic property. As shown in Figure 7c and in Supporting Information Figure S5, the structures of zigzag B edge passivated by two H with the average B−H bond length of 1.26 Å are similar to those of normal ZBNNR.

The electronic structure calculations show that the 2HB-BNNR with narrow zigzag section in the ground state exhibits the ferromagnetic metallic property. Interestingly, as the zigzag segment width continuously increases, the metallic → half-semiconducting → half-metallic behavior transitions are realized in 2HB-BNNR. Figure 7a, b, and d displays the band structures of 2HB-Z*m*-A12-BNNR with m = 2, 5, and 7 (see Figure S6 in the Supporting Information for other m), respectively. The bands δ for spin-up channel and δ' for spin-down channel across the Fermi level lead to the metallicity of 2HB-Z2-A12-BNNR (Figure 7a). When the m is increased from 2 to 5, the bands δ and δ' are shifted below and above the Fermi level (Figure 7b), respectively, resulting in the half-semiconducting property of hybrid ribbons with band gap of 3.11 eV for spin-up channel and 0.49 eV for spin-down channel. More interestingly, as the zigzag section width m is further increased to 7, the half metal is observed in 2HB-BNNR (Figure 7d), in which the spin-up channel is a semiconductor with a direct band gap of 3.11 eV, while the spin-down electrons show the metallic behavior. The larger half-metal gap is enough for the experimental manipulation of half-metallicity even at room temperature. The total DOS of 2HB-Z*m*-A12-BNNR (Figure 7e−g) also confirms the metallic → half-semiconducting → half-metallic behavior transitions. Such transitions are less affected by the armchair section width n (see Figure S7 in the Supporting Information). The strain change by

dx.doi.org/10.1021/jp405536x | J. Phys. Chem. C 2013, 117, 17309−17318

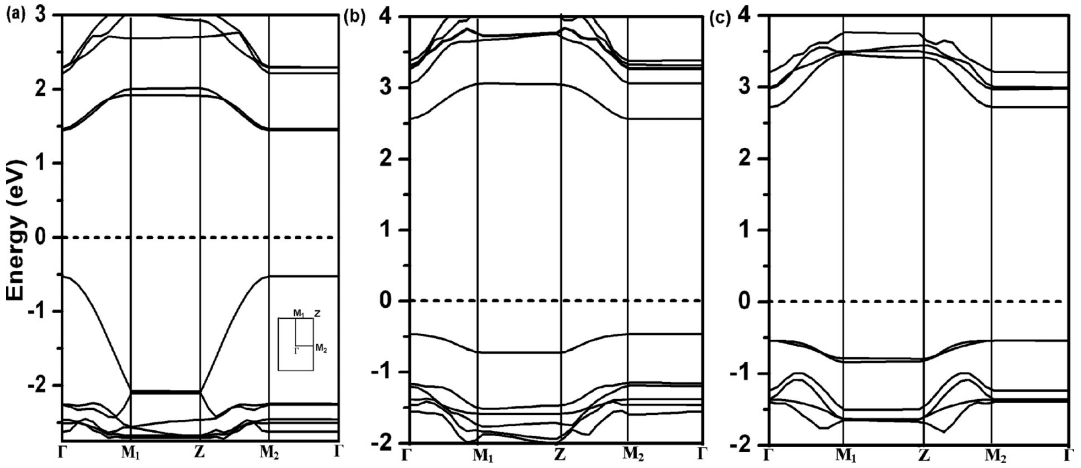

Figure 9. Band structures of hybrid BN sheet with (a) BG-N2-BN, (b) BG-NG-BN, and (c) NG-B2-BN. The inset in (a) shows the first Brillouin zone and special points for 2D hybrid BN sheet. The Fermi level is set to 0.

two H passivation in compressed zigzag edge may be responsible for the electronic property transitions.

To have insight into the magnetic properties of hybrid BNNR with two H-passivated B edge, the PDOS of zigzag edge B atoms and H and N atoms connecting the B edge of 2HB-Z*m*-A12-BNNR with m = 2, 5, and 7 (Figure 7e−g) and partial charge densities of δ and δ' bands of 2HB-Z2-A12-BNNR (Figure S3g and 3h in the Supporting Information) are displayed. The electrons in s orbital from two H passivating the B edge and in p_y orbital from N atoms nearest-neighbor the B edge of 2HB-Z*m*-A12-BNNR are spin polarized, leading to the magnetic moment of 1.2, 1.54, and 1.9 μ_B per unit cell for m = 2, 3, and 4−10, respectively. The spin densities of 2HB-Z5-A12-BNNR (Figure 7c) show that the induced magnetic moments are mainly located at the H and N connecting B edge other than at the edge B, which are also supported by the PDOS calculations (Figure 7e−g). Such results are due to that some electrons from the N and H atoms nearest-neighboring the B edge are transferred to the edge B atoms so that it forms four covalent bonds, resulting in the unpaired electrons located at these N and H atoms. Therefore, the magnetic properties of 2HB-BNNR are principally caused by the N and H atoms connecting the zigzag B edge.

3.4. 2D Hybrid BN Sheet. The 2D hybrid BN monolayer containing both normal zigzag and armchair section can be constructed by at least two 5−7 line defects. To form the hybrid BN sheet with only B-rich (N-rich) 5−7 line defect, as shown in Figure 8a and c, the antisite N (B) line defect must be introduced into the BN sheet, defined as BG-N2-BN (NG-B2-BN). In addition, the 5−7 line defects in BG-N2-BN (NG-B2-BN) present the mirror symmetry with respect to the antisite line defect as much as possible. In the absence of antisite N (B) line defect, the hybrid BN sheet is constructed by both B-rich and N-rich 5−7 line defect (Figure 8b), called BG-NG-BN. As shown in Figure 8a−c (side view) and Figure S8 in the Supporting Information, the geometrical structures reveal that the three types of hybrid BN sheet almost remain as the same planar structure with *h*-BN sheet, although the small out-of-plane structural distortion in BG-N2-BN along the x direction (Figure 8a) is found.

Figure 9a−c displays the calculated band structures of the hybrid BN sheet with BG-N2-BN, BG-NG-BN, and NG-B2-BN, respectively. The calculated results show that all hybrid BN sheets are semiconductors with direct band gaps of 1.97, 3.03, and 3.26 eV for BG-N2-BN, BG-NG-BN, and NG-B2-BN, respectively, which are significantly smaller than that of the perfect *h*-BN sheet with 4.77 eV. To understand the reduced band gap, the partial charge densities of VBM and CBM of hybrid BN sheet are calculated as shown in Figure 8d−g. The highest occupied state and lowest unoccupied state in BG-N2-BN sheet mainly consist of the bonding π orbital from the antisite N2 line defect and antibonding π orbital from the homoelemental B−B bond in 5−7 defect (Figure 8d and e), respectively. For BG-NG-BN (Figure 8f and g), the electronic states in VBM and CBM are mainly contributed by N and B atoms in 5−7 line defect, respectively. Therefore, the presence of defect state introduced by the 5−7 line defect and antisite line defect may be responsible for the reduction of band gap in BN sheet. The hybrid BN sheet constructed by GB may provide a novel way for BN-based semiconductor electronic devices.

4. CONCLUSION

In summary, we present the first-principles DFT calculations on the structural, electronic, and magnetic properties of hybrid BN nanoribbons and sheet, which are constructed by B-rich or N-rich GB with the 5−7 line defect joining the normal zigzag and armchair BN segments. Our results show that interesting electronic and magnetic properties are observed in hybrid BN nanostructures. The hybrid BN nanoribbons with H-passivated edge and sheet are nonmagnetic semiconductors with a reduced band gap as compared to prefect BN systems. The reduction of band gap in hybrid BN systems is attributed to the presence of line defect state. The band gap of H-passivated hybrid BNNR constructed by B-rich GB exhibits a dependence on area, while the ribbon width has less influence on the band gap of hybrid ribbons with N-rich GB. The armchair-zigzag BNNR created by B-rich GB with bare zigzag N edge are always half-semiconductors with the ferromagnetic (FM) ground state, whereas the antiferromagnetic → nonmagnetic semiconductor transition in hybrid BN ribbons with bare B edge occurred when the narrow zigzag segment is changed to the wider one. Interestingly, totally different from the perfect zigzag BNNR, the hybrid BNNR with two-H-terminated B edge exhibits the metallic → half-semiconducting → half-metallic behavior transitions as its number of the zigzag BN chains gradually

dx.doi.org/10.1021/jp405536x | J. Phys. Chem. C 2013, 117, 17309−17318

increases due to the compressed zigzag edge. Therefore, the hybrid BN nanomaterials constructed by GB with 5−7 line defects provide potential applications for BN-based nanoelectronic and spintronic devices.

■ ASSOCIATED CONTENT

Supporting Information

Band structures, partial charge densities, and optimized structures for other hybrid BNNR and other AIMD simulations. This material is available free of charge via the Internet at http://pubs.acs.org.

■ AUTHOR INFORMATION

Corresponding Author

*Fax: +86-797-8393536. E-mail: tsb1980@xmu.edu.cn.

Notes

The authors declare no competing financial interest.

■ ACKNOWLEDGMENTS

This work was supported by the National Science Foundation of China (21103026). We acknowledge simulating discussions with Z. Cao and are thankful for the computational resources and assistance provided by the State Key Laboratory of Physical Chemistry of Solid Surfaces (Xiamen University).

■ REFERENCES

(1) Kubota, Y.; Watanabe, K.; Tsuda, O.; Taniguchi, T. Deep Ultraviolet Light-Emitting Hexagonal Boron Nitride Synthesized at Atmospheric Pressure. *Science* **2007**, *317*, 932−934.

(2) Zhang, Y.; Tan, Y.-W.; Stormer, H. L.; Kim, P. Experimental Observation of the Quantum Hall Effect and Berry's Phase in Graphene. *Nature* **2005**, *438*, 201−204.

(3) Novoselov, K. S.; Jiang, D.; Schedin, F.; Booth, T. J.; Khotkevich, V. V.; Morozov, S. V.; Geim, A. K. Two-Dimensional Atomic Crystals. *Proc. Natl. Acad. Sci. U.S.A.* **2005**, *102*, 10451−10453.

(4) Nag, A.; Raidongia, K.; Hembram, K. P. S. S.; Datta, R.; Waghmare, U. V.; Rao, C. N. Graphene Analogues of BN: Novel Synthesis and Properties. *ACS Nano* **2010**, *4*, 1539−1544.

(5) Golberg, D.; Bando, Y.; Huang, Y.; Terao, T.; Mitome, M.; Tang, C.; Zhi, C. Boron Nitride Nanotubes and Nanosheets. *ACS Nano* **2010**, *4*, 2979−2993.

(6) Tang, S.; Cao, Z. Structural and Electronic Properties of the Fully Hydrogenated Boron Nitride Sheets and Nanoribbons: Insight from First-principles Calculations. *Chem. Phys. Lett.* **2010**, *488*, 67−72.

(7) Tang, S.; Yu, J.; Liu, L. Tunable Doping and Band Gap of Graphene on Functionalized Hexagonal Boron Nitride with Hydrogen and Fluorine. *Phys. Chem. Chem. Phys.* **2013**, *15*, 5067−5077.

(8) Zhou, J.; Wang, Q.; Sun, Q.; Jena, P. Electronic and Magnetic Properties of a BN Sheet Decorated with Hydrogen and Fluorine. *Phys. Rev. B* **2010**, *81*, 085442.

(9) Du, A. J.; Smith, S. C.; Lu, G. Q. First-Principle Studies of Electronic Structure and C-Doping Effect in Boron Nitride Nanoribbon. *Chem. Phys. Lett.* **2007**, *447*, 181−186.

(10) Nakamura, J.; Nitta, T.; Natori, A. Electronic and Magnetic Properties of BNC Ribbons. *Phys. Rev. B* **2005**, *72*, 205429.

(11) Park, C.-H.; Louie, S. G. Energy Gaps and Stark Effect in Boron Nitride Nanoribbons. *Nano Lett.* **2008**, *8*, 2200−2203.

(12) Zhang, Z.; Guo, W. Energy-Gap Modulation of BN Ribbons by Transverse Electric Fields: First-Principles Calculations. *Phys. Rev. B* **2008**, *77*, 075403.

(13) Qi, J.; Qian, X.; Qi, L.; Feng, J.; Shi, D.; Li, J. Strain-Engineering of Band Gaps in Piezoelectric Boron Nitride Nanoribbons. *Nano Lett.* **2012**, *12*, 1224−1228.

(14) Zheng, F.; Zhou, G.; Liu, Z.; Wu, J.; Duan, W.; Gu, B.-L.; Zhang, S. B. Half Metallicity along the Edge of Zigzag Boron Nitride Nanoribbons. *Phys. Rev. B* **2008**, *78*, 205415.

(15) Lai, L.; Lu, J.; Wang, L.; Luo, G.; Zhou, J.; Qin, R.; Gao, Z.; Mei, W. N. Magnetic Properties of Fully Bare and Half-Bare Boron Nitride Nanoribbons. *J. Phys. Chem. C* **2009**, *113*, 2273−2276.

(16) Chen, W.; Li, Y.; Yu, G.; Li, C.-Z.; Zhang, S. B.; Zhou, Z.; Chen, Z. Graphane/Fluorographene Bilayer: Considerable C−H···F−C Hydrogen Bonding and Effective Band Structure Engineering. *J. Am. Chem. Soc.* **2012**, *134*, 11269−11275.

(17) Wang, Y.; Ding, Y.; Ni, J. Fluorination-Induced Half-Metallicity in Zigzag Boron Nitride Nanoribbons: First-Principles Calculations. *Phys. Rev. B* **2010**, *81*, 193407.

(18) Barone, V.; Peralta, J. E. Magnetic Boron Nitride Nanoribbons with Tunable Electronic Properties. *Nano Lett.* **2008**, *8*, 2210−2214.

(19) Ding, Y.; Wang, Y.; Ni, J. The Stabilities of Boron Nitride Nanoribbons with different Hydrogen-Terminated Edges. *Appl. Phys. Lett.* **2009**, *94*, 233107.

(20) Tang, S.; Cao, Z. Carbon-Doped Zigzag Boron Nitride Nanoribbons with Widely Tunable Electronic and Magnetic Properties: Insight from Density Functional Calculations. *Phys. Chem. Chem. Phys.* **2010**, *12*, 2313−2320.

(21) Lahiri, J.; Lin, Y.; Bozkurt, P.; Oleynik, I. I.; Batzill, M. An Extended Defect in Graphene as A Metallic Wire. *Nat. Nanotechnol.* **2010**, *5*, 326−329.

(22) Yazyev, O. V.; Louie, S. G. Electronic Transport in Polycrystalline Graphene. *Nat. Mater.* **2010**, *9*, 806−809.

(23) Alexandre, S. S.; Lúcio, A. D.; Neto, A. H. C.; Nunes, R. W. Correlated Magnetic States in Extended One-Dimensional Defects in Graphene. *Nano Lett.* **2012**, *12*, 5097−5102.

(24) Zhou, J.; Hu, T.; Dong, J.; Kawazoe, Y. Ferromagnetism in a Graphene Nanoribbon with Grain Boundary Defects. *Phys. Rev. B* **2012**, *86*, 035434.

(25) Botello-Méndez, A. R.; Cruz-Silva, E.; López-Urías, F.; Sumpter, B. G.; Meunier, V.; Terrones, M.; Terrones, H. Spin Polarized Conductance in Hybrid Graphene Nanoribbons Using 5−7 Defects. *ACS Nano* **2009**, *3*, 3606−3612.

(26) Auwärter, W.; Muntwiler, M.; Osterwalder, J.; Greber, T. Defect Lines and Two-Domain Structure of Hexagonal Boron Nitride Films on Ni(111). *Surf. Sci. Lett.* **2003**, *545*, L735−L740.

(27) Kim, K. K.; Hsu, A.; Jia, X.; Kim, S. M.; Shi, Y.; Hofmann, M.; Nezich, D.; Rodriguez-Nieva, J. F.; Dresselhaus, M.; Palacios, T.; Kong, J. Synthesis of Monolayer Hexagonal Boron Nitride on Cu Foil Using Chemical Vapor Deposition. *Nano Lett.* **2012**, *12*, 161−166.

(28) Liu, Y.; Zou, X.; Yakobson, B. I. Dislocations and Grain Boundaries in Two-Dimensional Boron Nitride. *ACS Nano* **2012**, *6*, 7053−7058.

(29) Gomes, L. C.; Alexandre, S. S.; Chacham, H.; Nunes, R. W. Stability of Edges and Extended Defects on Boron Nitride and Graphene Monolayers: The Role of Chemical Environment. *J. Phys. Chem. C* **2013**, *117*, 11770−11779.

(30) Li, X.; Wu, X.; Zeng, X. C.; Yang, J. Band-Gap Engineering via Tailored Line Defects in Boron-Nitride Nanoribbons, Sheets, and Nanotubes. *ACS Nano* **2012**, *6*, 4104−4112.

(31) Yamijala, S. S.; Pati, S. K. Electronic and Magnetic Properties of Zigzag Boron-Nitride Nanoribbons with Even and Odd-Line Stone-Wales (5−7 Pair) Defects. *J. Phys. Chem. C* **2013**, *117*, 3580−3594.

(32) Kresse, G.; Hafner, J. Ab Initio Molecular Dynamics for Liquid Metals. *Phys. Rev. B* **1993**, *47*, 558−561.

(33) Perdew, J. P.; Wang, Y. Accurate and Simple Analytic Representation of the Electron-Gas Correlation Energy. *Phys. Rev. B* **1992**, *45*, 13244−13249.

(34) Perdew, J. P.; Burke, K.; Ernzerhof, M. Generalized Gradient Approximation Made Simple. *Phys. Rev. Lett.* **1996**, *77*, 3865−3868.

(35) Nakada, K.; Fujita, M.; Dresselhaus, G.; Dresselhaus, M. S. Edge State in Graphene Ribbons: Nanometer Size Effect and Edge Shape Dependence. *Phys. Rev. B* **1996**, *54*, 17954−17961.

(36) Tang, S.; Cao, Z. Theoretical Study of Stabilities and Electronic Properties of the Vacancy and Carbon-doping Defects in Zigzag Boron Nitride Nanoribbons. *Comput. Mater. Sci.* **2010**, *48*, 648−654.

(37) Cervantes-Sodi, F.; Csányi, G.; Piscanec, S.; Ferrari, A. C. Edge-Functionalized and Substitutionally Doped Graphene Nanoribbons: Electronic and Spin Properties. *Phys. Rev. B* **2008**, *77*, 165427.
(38) Son, Y.-W.; Cohen, M. L.; Louie, S. G. Energy Gaps in Graphene Nanoribbons. *Phys. Rev. Lett.* **2006**, *97*, 216803.